



**HAL**  
open science

## Laser desorption ionization time-of-flight mass spectrometry of $GexSe_{1-x}$ chalcogenide glasses, their thin films, and GeSe mixtures

R. Mawale, T. Halenkovič, M. Bouška, J. Gutwirth, Virginie Nazabal, V. Takáts, A. Csík, J. Havel, L. Prokeš, P. Němec

### ► To cite this version:

R. Mawale, T. Halenkovič, M. Bouška, J. Gutwirth, Virginie Nazabal, et al.. Laser desorption ionization time-of-flight mass spectrometry of  $GexSe_{1-x}$  chalcogenide glasses, their thin films, and GeSe mixtures. *Journal of Non-Crystalline Solids*, 2019, 509, pp.65-73. 10.1016/j.jnoncrysol.2018.12.020 . hal-02051158

**HAL Id: hal-02051158**

**<https://univ-rennes.hal.science/hal-02051158>**

Submitted on 16 Jun 2021

**HAL** is a multi-disciplinary open access archive for the deposit and dissemination of scientific research documents, whether they are published or not. The documents may come from teaching and research institutions in France or abroad, or from public or private research centers.

L'archive ouverte pluridisciplinaire **HAL**, est destinée au dépôt et à la diffusion de documents scientifiques de niveau recherche, publiés ou non, émanant des établissements d'enseignement et de recherche français ou étrangers, des laboratoires publics ou privés.

This is the accepted version of the following article

Ravi Mawale, Tomáš Halenkovič, Marek Bouška, Jan Gutwirth, Virginie Nazabal, Viktor Takáts, Attila Csík, Josef Havel, Lubomír Prokeš, Petr Němec (2019). Laser desorption ionization time-of-flight mass spectrometry of GexSe1-x chalcogenide glasses, their thin films, and Ge:Se mixtures. *Journal of Non-Crystalline Solids*. DOI: 10.1016/j.jnoncrysol.2018.12.020

This accepted version is available from URI <https://hdl.handle.net/10195/75017>

Publisher's version is available from:

<https://www.sciencedirect.com/science/article/pii/S0022309319300365>



This version is licenced under a [Creative Commons Attribution-NonCommercial-NoDerivatives 4.0 International](https://creativecommons.org/licenses/by-nc-nd/4.0/).

# Laser Desorption Ionization Time-of-Flight Mass Spectrometry of $\text{Ge}_x\text{Se}_{1-x}$ Chalcogenide Glasses, Their Thin Films, and Ge:Se Mixtures

Ravi Mawale<sup>1</sup>, Tomáš Halenkovič<sup>1,2</sup>, Marek Bouška<sup>1</sup>, Jan Gutwirth<sup>1</sup>, Virginie Nazabal<sup>1,2</sup>, Viktor Takáts<sup>3</sup>, Attila Csík<sup>3</sup>, Josef Havel<sup>4</sup>, Lubomír Prokeš<sup>4,5,6</sup>, Petr Němec<sup>1\*</sup>

<sup>1</sup>Department of Graphic Arts and Photophysics, Faculty of Chemical Technology, University of Pardubice, Studentská 573, 53210 Pardubice, Czech Republic

<sup>2</sup>Institut des Sciences Chimiques de Rennes, UMR-CNRS 6226, Equipe Verres et Céramiques, Université de Rennes 1, 35042 Rennes, France

<sup>3</sup>Institute for Nuclear Research (ATOMKI), Hungarian Academy of Sciences, Bem tér 18/C, H-4026 Debrecen, Hungary

<sup>4</sup>Department of Chemistry, Faculty of Science, Masaryk University, Kamenice 5/A14, 625 00 Brno, Czech Republic

<sup>5</sup>Department of Physical Electronics, Faculty of Science, Masaryk University, Kotlářská 2, 61137 Brno, Czech Republic

<sup>6</sup>CEPLANT, R&D Centre for Low-Cost Plasma and Nanotechnology Surface Modification, Masaryk University, Kotlářská 2, 61137 Brno, Czech Republic

**\* Author to whom correspondence should be addressed.**

Address reprint request to: Petr Nemeč, Email: [petr.nemec@upce.cz](mailto:petr.nemec@upce.cz), Phone: +420466038502

University of Pardubice, Studentská 573, 53210 Pardubice, Czech Republic

**Keywords:** Chalcogenide glasses; Thin films; Laser desorption ionization; Time-of-Flight mass spectrometry; Clusters

## 1. Introduction

Amorphous chalcogenides (as bulk glasses, fibers, and thin film) have been extensively studied due to their excellent infrared transparency, high linear and nonlinear refractive indices, and ease of processing [1]. Hence they are widely applied in infrared technology, integrated and non-linear optics. Chalcogenides are also used for the fabrication of optical phase change memories, in photolithography, holography, optical switching, laser written waveguides, photonic crystals, etc.[2–4].

In binary systems, arsenic-based chalcogenide glasses are considered as prototype chalcogenide glasses due to their broad glass-forming region. However, the toxicity of the arsenic limits their use for the environmental concern. Contrary, germanium-based chalcogenide glasses could be considered as a potential alternative, due to the advantages of their relatively higher stability, environmental sustainability, and glass forming ability. Germanium-based chalcogenide glasses, especially germanium selenides show good mechanical properties, such as hardness, adhesion, low internal stress, and water resistance [5].

Germanium-based selenide glasses are commonly preferred over to germanium-based sulfides or tellurides due to their mid-IR transparency and large (non)linear refractive indices. As a consequence of these interesting properties,  $\text{Ge}_x\text{Se}_{1-x}$  glasses are investigated for the study of glass forming region, structure, physical properties, kinetics of the glass transition, thermoelectric properties, etc. [5,6,15–17,7–14]. Many different techniques are employed for the characterization of Ge-Se system glasses and thin films including infrared spectroscopy, Raman scattering spectroscopy, NMR spectroscopy, etc. [18–23]. However, mass spectrometric studies of Ge-Se system are limited and require more attention.

Laser desorption/ionization with Time-of-Flight mass spectrometry (LDI TOFMS) has been considered as a promising technique for the generation and study of clusters of various solid materials including chalcogenide glasses. It has been shown that this technique can be used to elucidate the structural fragments present in the plasma after high-energy pulsed laser irradiation of chalcogenide glasses in bulk as well as thin film forms [24–29].

The aim of this work was to investigate chalcogenide glasses from Ge-Se system ( $\text{Ge}_{0.1}\text{Se}_{0.9}$ ,  $\text{Ge}_{0.2}\text{Se}_{0.8}$ ,  $\text{Ge}_{0.3}\text{Se}_{0.7}$ , and  $\text{Ge}_{0.33}\text{Se}_{0.67}$ ) and corresponding thin films using LDI TOFMS analysis. The resulting information provide better understanding of the structural fragments present in the plasma generated via the pulsed laser irradiation of the solid-state material. Further, we also performed a comparison of the species generated from different mixtures of elemental Ge and Se with Ge-Se glasses (with and without being dispersed in the parafilm) and thin films. Finally, we used secondary neutral mass spectrometry (SNMS) for the characterization of  $\text{Ge}_x\text{Se}_{1-x}$  glasses and their thin films.

## **2. Materials and methods**

### *2.1. Chemicals*

Germanium, selenium (both 5N purity), methanol and acetonitrile were purchased from Sigma-Aldrich (Steinheim, Germany). Xylene (a mixture of isomers) was purchased from Mikrochem Spol. s. r. o. (Pezinok, Slovak Republic) and parafilm from Pechiney Plastic Packaging (Chicago, IL, USA). Micro-90 (cleaning agent) was from Kratos (Manchester, UK). Silicon wafers used as substrates for the thin films deposition were purchased from ON SEMICONDUCTORS (Czech Republic). Deionized water was distilled once in glass and then double distilled from a quartz apparatus Heraeus

Quarzschnmelze (Hanau, Germany) to produce ultrapure water. All the other reagents were of analytical grade purity.

## *2.2. Mixtures of Ge and Se*

An appropriate amount of high purity elemental germanium and selenium were weighed and mixed together. The mixture was then suspended in acetonitrile and ultrasound for 1 min before deposited on a target plate for mass spectrometric measurements.

## *2.3. Bulk glass synthesis*

Chalcogenide glasses ( $\text{Ge}_{0.1}\text{Se}_{0.9}$ ,  $\text{Ge}_{0.2}\text{Se}_{0.8}$ ,  $\text{Ge}_{0.3}\text{Se}_{0.7}$ , and  $\text{Ge}_{0.33}\text{Se}_{0.67}$ ) were synthesized from high purity elements mentioned above using the conventional melting and quenching technique [30].

## *2.4. Preparation of thin films*

Amorphous thin films of  $\text{Ge}_{0.2}\text{Se}_{0.8}$  and  $\text{Ge}_{0.33}\text{Se}_{0.67}$  were deposited using conventional rf (13.56 MHz) magnetron sputtering technique. The experimental conditions of the deposition process are described elsewhere [31]. For the deposition of the  $\text{Ge}_{0.33}\text{Se}_{0.67}$  thin film, commercial 2'' sputtering target (American Elements Corp., Los Angeles, CA, USA) was exploited. The  $\text{Ge}_{0.2}\text{Se}_{0.8}$  sputtering target was prepared by conventional melt-quenching technique [30].

# **3. Experimental**

## *3.1. Ellipsometry*

Optical functions (spectral dependencies of extinction coefficient and refractive index), as well as thicknesses of prepared thin films, were obtained from the analysis of spectroscopic ellipsometry data measured using an ellipsometry with an automatic rotating analyzer (VASE, J. A. Woollam Co., Inc.).

### *3.2. Scanning Electron Microscopy and Energy Dispersive X-ray Spectroscopy*

A scanning electron microscope (SEM) with an energy dispersive X-ray analyzer (EDS, TESCAN VEGA 3 EasyProbe) was used for the study of surface morphology and determination of chemical composition of fabricated materials. The uncertainty of EDS measurements for studied glasses and films is  $\pm 1$  at. %. Typically, the EDS measurements were performed at 3 spots per sample and averaged.

### *3.3. LDI TOF Mass spectrometry*

Prior to each LDI TOFMS measurement, the target plate was cleaned according to the Shimadzu target cleaning protocol. Specifically, it includes cleaning with water, then sonicated in Micro-90 cleaning agent solution for 15 min and finally rinsed several times with water and methanol.

Chalcogenide bulk materials were powdered with agate mortar and pastel. Then, 1  $\mu$ L of acetonitrile suspension of the sample powder (1 mg/mL) was deposited on the target plate and dried in a stream of air at room temperature and LDI TOF mass spectra were recorded. Thin films were fixed on the target plate using adhesive tape and then measured.

Mass spectra were acquired using AXIMA Resonance mass spectrometer from Kratos Analytical Ltd. (Manchester, UK). The instrument details are given in [26]. The laser energy varied in arbitrary units (a. u.) from 0 to 180; this relative scale is used hereafter.

The exposed sample spot size was approximately 150  $\mu\text{m}$  in diameter, giving the laser energy fluence  $\sim 1 \text{ J cm}^{-2}$ . Mass spectra were measured in both, positive and negative ion modes by accumulating the data from at least 2000 laser shots. External calibration in individual  $m/z$  ranges was done using red phosphorus clusters [32], while the accuracy achieved was below  $\pm 30 \text{ mDa}$ .

Theoretical isotopic patterns were calculated using Launchpad software (Kompact version 2.9.3, 2011) from Kratos Analytical Ltd. (Manchester, UK).

#### 3.4. *Secondary neutral mass spectrometry*

Secondary neutral mass spectra measurements were carried out on INA-X type Secondary Neutral Mass Spectrometer produced by SPECS GmbH, Berlin [33]. The surface bombardment and post-ionization of sputtered neutral particles were done by the Electron Cyclotron Wave Resonance argon plasma. The SNMS was operated in high-frequency mode which insured effective charge compensation against surface charge accumulation and thus results in a homogeneous ion bombardment. The  $-450 \text{ V}$  sputtering potential at 100 kHz frequency with 80% duty cycle was applied on a sample surface.  $\text{Ar}^+$  ions are extracted from low-pressure plasma with a current density of  $\sim 1 \text{ mA/cm}^2$ . The sputtered area was confined to a circle of 3 mm in diameter by a Ta mask. Post-ionized neutral particles are directed into a quadruple mass spectrometer Balzers QMA 410 by electrostatic lenses. SNMS data were recorded for  $\text{Ge}_{0.1}\text{Se}_{0.9}$ ,  $\text{Ge}_{0.2}\text{Se}_{0.8}$ ,  $\text{Ge}_{0.3}\text{Se}_{0.7}$ , and  $\text{Ge}_{0.33}\text{Se}_{0.67}$  bulk glasses,  $\text{Ge}_{0.2}\text{Se}_{0.8}$  and  $\text{Ge}_{0.33}\text{Se}_{0.67}$  thin films.

## 4. Results and Discussion

The morphology of the thin films was determined by SEM and the average composition of fabricated glasses/thin films was obtained by EDS when measuring at different positions on the bulk glass materials/thin films. A good agreement between nominal and measured chemical composition was obtained; typically a slight over-stoichiometry of germanium (up to 2 at.%) at maximum was evidenced for the bulk glass materials. The morphology of the layers is of good quality as results from SEM micrographs (Supplementary Fig. S1).

The thickness ( $\pm 2$  nm) of the deposited films ( $\text{Ge}_{0.2}\text{Se}_{0.8}$  and  $\text{Ge}_{0.33}\text{Se}_{0.67}$ ) was found to be  $\sim 990$  and  $\sim 1290$  nm, as determined by VASE data analysis. Furthermore, optical functions and optical bandgap ( $E_g^{opt}$ ) values were obtained from VASE data using Cody-Lorentz oscillator model which is suitable for the description of amorphous chalcogenides [33–35].  $E_g^{opt}$  ( $\pm 0.01$  eV) was found to be 2.06 and 1.97 eV for  $\text{Ge}_{0.33}\text{Se}_{0.67}$  and  $\text{Ge}_{0.2}\text{Se}_{0.8}$  films respectively. Corresponding refractive indices at 1550 nm ( $\pm 0.01$ ) are 2.44 and 2.38.

LDI TOFMS characterization of Ge-Se elemental mixtures, powdered glasses ( $\text{Ge}_{0.1}\text{Se}_{0.9}$ ,  $\text{Ge}_{0.2}\text{Se}_{0.8}$ ,  $\text{Ge}_{0.3}\text{Se}_{0.7}$ , and  $\text{Ge}_{0.33}\text{Se}_{0.67}$ ), and thin films (deposited from  $\text{Ge}_{0.2}\text{Se}_{0.8}$  and  $\text{Ge}_{0.33}\text{Se}_{0.67}$  targets) was performed in both, positive and negative ion modes with the aim to assess the stoichiometry of the generated positively and negatively charged  $\text{Ge}_a\text{Se}_b^\pm$  cluster ions. The stoichiometry of the clusters was determined by comparing the experimental and theoretical isotopic patterns. We noticed that when the

number of Ge and/or Se atoms increased in the clusters, the isotopic envelopes are complex due to close atomic masses of Ge and Se (72.64 and 78.94, respectively).

The mass spectra were obtained at varied laser energy by its systematical increase to understand the influence of laser energy on the generation of clusters. The threshold energy value for the generation of ions from Ge-Se elemental mixtures, glasses, and thin films was evaluated for both positive and negative ion modes. At higher laser energies, the signal intensities of the generated clusters gradually climbed. The mass spectra with sufficient mass resolution and the highest number of detected clusters in both, negative and positive ion modes were recorded and used for data processing.

#### 4.1. Ge:Se elemental mixtures

Firstly, the elemental mixtures of Ge and Se with five different molar ratios (1:3, 1:1, 3:1, 5:1, and 10:1) were prepared and examined *via* LDI TOFMS. In the positive ion mode, the mass spectra obtained from Ge:Se 3:1 and 1:3 precursors show the presence of  $\text{Se}_b^+$  ( $b=2-9$ ) species, while for 1:1 mixture  $\text{Se}_b^+$  ( $b=2-7$ ) clusters were detected. Few  $\text{Ge}_a\text{Se}_b^+$  ( $\text{GeSe}_2^+$  and  $\text{GeSe}_4^+$ ) clusters were also identified. These  $\text{Ge}_a\text{Se}_b^+$  clusters are overlapped with two or more different species. In the case of Ge:Se 3:1 mixture where Ge is in excess,  $\text{GeSe}_2^+$  (75%) +  $\text{Se}_3^+$  (25%),  $\text{GeSe}_4^+$  (15%) +  $\text{Se}_5^+$  (85%), and  $\text{GeSe}_5^+$  (40%) +  $\text{Se}_6^+$  (60%) species were detected. The percentage in brackets indicates the contribution of individual species to the overall peak intensity. No more clusters were identified over range  $m/z$  800. It was observed that varying the laser energy, the isotopic patterns of some species can be different depending upon the percentual contribution of individual species. One such an example is given in Supplementary Fig. S2 which presents the difference of isotopic patterns obtained from Ge:Se (3:1) mixture at different laser energies. Even for samples Ge:Se 5:1 and 10:1 with high excess of germanium,

unary  $\text{Se}_b^+$  ( $b=2-9$ ) and  $\text{Se}_b^+$  ( $b=2-8$ ) clusters were detected. In addition, many  $\text{Ge}_a\text{Se}_b^+$  clusters were identified (Supplementary Table 1). Several germanium rich clusters  $\text{Ge}_4^+$ ,  $\text{Ge}_4\text{Se}^+$ ,  $\text{Ge}_5\text{Se}^+$  (35%) +  $\text{Ge}_4\text{Se}_2^+$  (65%),  $\text{Ge}_5\text{Se}_2^+$  (40%) +  $\text{Ge}_4\text{Se}_3^+$  (60%), and  $\text{Ge}_5\text{Se}_3^+$  (80%) +  $\text{Ge}_4\text{Se}_4^+$  (20%) were detected. Mass spectra of Ge:Se 5:1 mixture in different mass ranges are illustrated in Fig. 1. We note that AXIMA Resonance QIT TOFMS allows to measure mass spectra in different  $m/z$  ranges; some parts of the  $m/z$  ranges are common in two consecutive ranges due to this fact. It was observed that the species obtained in the common parts of the  $m/z$  ranges show different isotopic patterns which correspond to the same/different species with different contribution of individual species to the overall isotopic pattern.

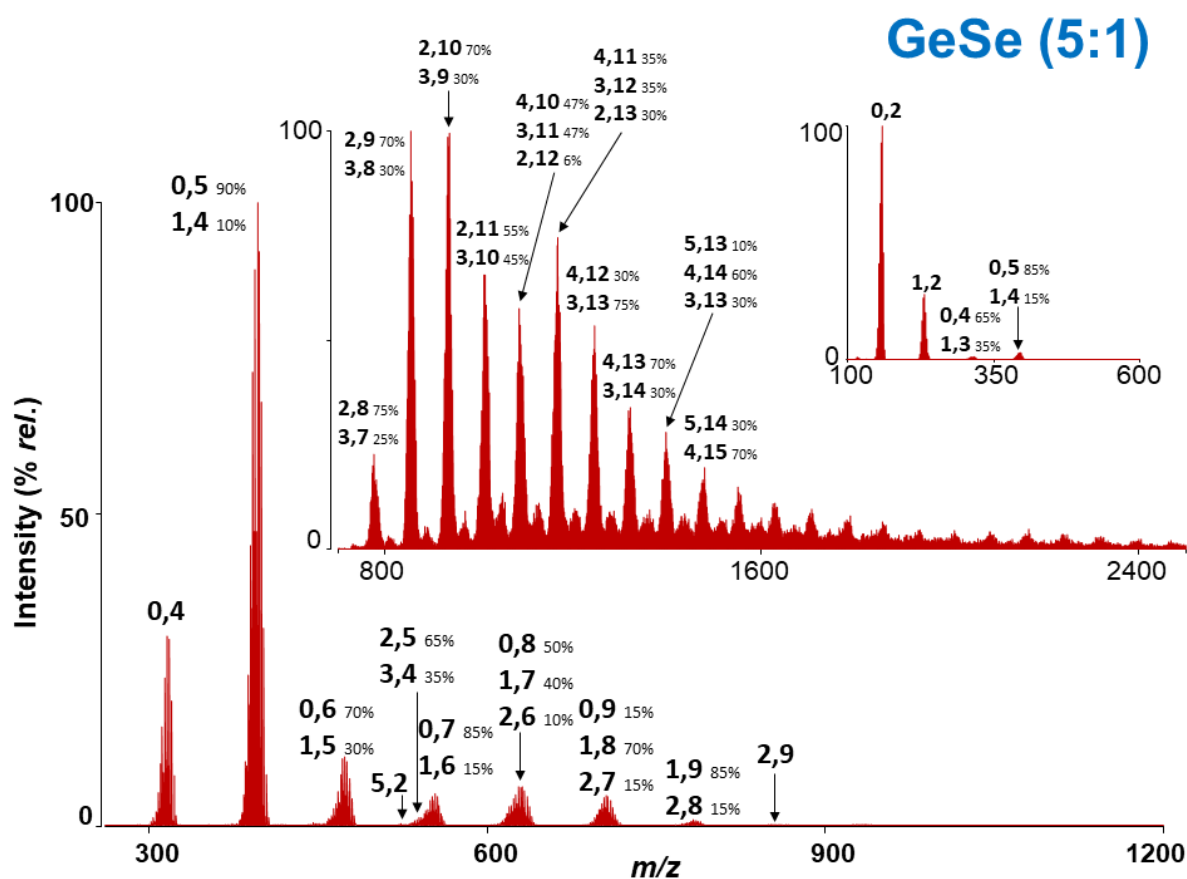


**Fig. 1:** Mass spectra obtained from Ge:Se (5:1) mixture. Conditions: positive ion mode, laser energy 160 a.u.

In the negative ion mode, the “richest” mass spectra with the highest number of clusters, peak intensities, and sufficient mass resolution were obtained at laser energy  $\sim 140$ - $150$  a.u. The lowest mass species observed is  $\text{Se}_2^-$  one. The most intensive peaks in the mass spectra are  $\text{Se}_2^-$ ,  $\text{Se}_3^-$ , and  $\text{Se}_4^-$ . The heaviest cluster identified for all the samples is  $\text{Ge}_3\text{Se}_9^-$  overlapped with  $\text{Ge}_2\text{Se}_{10}^-$ . Like in the positive ion mode, most of the isotopic patterns are complex due to the overlapping of two or more species with each other. This overlapping is due to close atomic masses of Ge and Se, hence as the number of Ge and Se atoms in the clusters increases, the isotopic patterns get more complex. However, at achieved mass resolution most of the species were identified. Mass spectra obtained from Ge:Se 10:1 are given in the Supplementary Fig. S3. Many germanium rich clusters such as  $\text{Ge}_4\text{Se}_b^-$  ( $b = 0$ - $3$ );  $\text{Ge}_6\text{Se}_b^-$  ( $b = 0$ - $3$ );  $\text{Ge}_3\text{Se}_2^-$ ;  $\text{Ge}_7^-$  were detected below  $m/z$  700. No more clusters were detected above  $m/z$  2000, while the clusters observed in the range  $m/z$  1500-2000 are of low intensity and they are difficult to identify.

#### 4.2. Ge-Se glasses and thin films

In this section, we deal with the LDI TOFMS of bulk  $\text{Ge}_{1-x}\text{Se}_x$  glasses and their sputtered thin films. We applied a similar methodology which we used for the Ge-Se elemental mixtures. The influence of laser energy on the generation of plasma species was studied; it was found that the ionization of positively charged ions started when the energy reached 120 a.u. Increasing the laser energy, the intensities of the ions gradually climbed up to 160 a.u., a further increase in laser energy decreases the intensities (specifically of higher mass clusters). In positive ion mode, the “richest” mass spectra with respect to the higher number of clusters, greater intensities, and sufficient mass resolution were obtained at laser energy about 140-160 a.u. The lowest mass cluster

assigned (at measurement conditions) was  $\text{Se}_2^+$  for all the glass samples and the highest mass cluster detected was  $\text{Ge}_7\text{Se}_{16}^+$  (50%) +  $\text{Ge}_6\text{Se}_{17}^+$  (50%) for  $\text{Ge}_{0.1}\text{Se}_{0.9}$ ; however, the intensity of this highest mass cluster was quite low as compared to  $\text{Se}_2^+$ . Several series of clusters with increasing number of Ge and Se atoms were detected:  $\text{GeSe}_b^+$  ( $b = 2-9$ );  $\text{Ge}_2\text{Se}_b^+$  ( $b = 3-11$ );  $\text{Ge}_3\text{Se}_b^+$  ( $b = 4-13$ );  $\text{Ge}_4\text{Se}_b^+$  ( $b = 5-15$ );  $\text{Ge}_5\text{Se}_b^+$  ( $b = 7-17$ );  $\text{Ge}_6\text{Se}_b^+$  ( $b = 8-17$ );  $\text{Ge}_7\text{Se}_b^+$  ( $b = 10-16$ );  $\text{Ge}_8\text{Se}_b^+$  ( $b = 13-14$ ). In total, the number of species detected for all four samples are: 47 for  $\text{Ge}_{0.1}\text{Se}_{0.9}$ , 57 for  $\text{Ge}_{0.2}\text{Se}_{0.8}$ , 55 for  $\text{Ge}_{0.3}\text{Se}_{0.7}$ , and 55 for  $\text{Ge}_{0.33}\text{Se}_{0.67}$ . Several low-intensity  $\text{Ge}_a\text{Se}_b^+$  species were observed but due to the insufficient mass resolution, the stoichiometry of these clusters was not determined. In addition to the above-mentioned clusters, one  $\text{Ge}_5^+$  and several other germanium rich clusters  $\text{Ge}_4\text{Se}^+$ ,  $\text{Ge}_4\text{Se}_2^+$ ,  $\text{Ge}_5\text{Se}^+$ ,  $\text{Ge}_5\text{Se}_2^+$ ,  $\text{Ge}_5\text{Se}_3^+$ ,  $\text{Ge}_6\text{Se}_2^+$ ,  $\text{Ge}_6\text{Se}_3^+$ , and  $\text{Ge}_7\text{Se}_2^+$  were detected (Supplementary Table 2); the intensity of these Ge rich clusters was quite low as compared to the Se rich clusters. Comparison of mass spectra obtained for all four glass samples is given in Fig. 2; for simplicity, the stoichiometries of the clusters for only one sample are shown. Similarly, as discussed in the previous part, most of the isotopic patterns were overlapped with  $\geq 2$  species; however, their individual contribution to the overall isotopic pattern is different. Fig. 3 presents an example of a comparison of experimental and model isotopic patterns together with the overlap of the individual species and their contribution to the overall isotopic pattern. Few oxygenated carbon clusters were detected in the mass range  $m/z$  1100-1250. The intensities of these clusters gradually decreased from  $\text{Ge}_{0.1}\text{Se}_{0.9}$  to  $\text{Ge}_{0.33}\text{Se}_{0.67}$  as the content of selenium decreased in the bulk samples. This might indicate that carbon and oxygen impurities originate from the selenium precursor used for the preparation of bulk glasses.

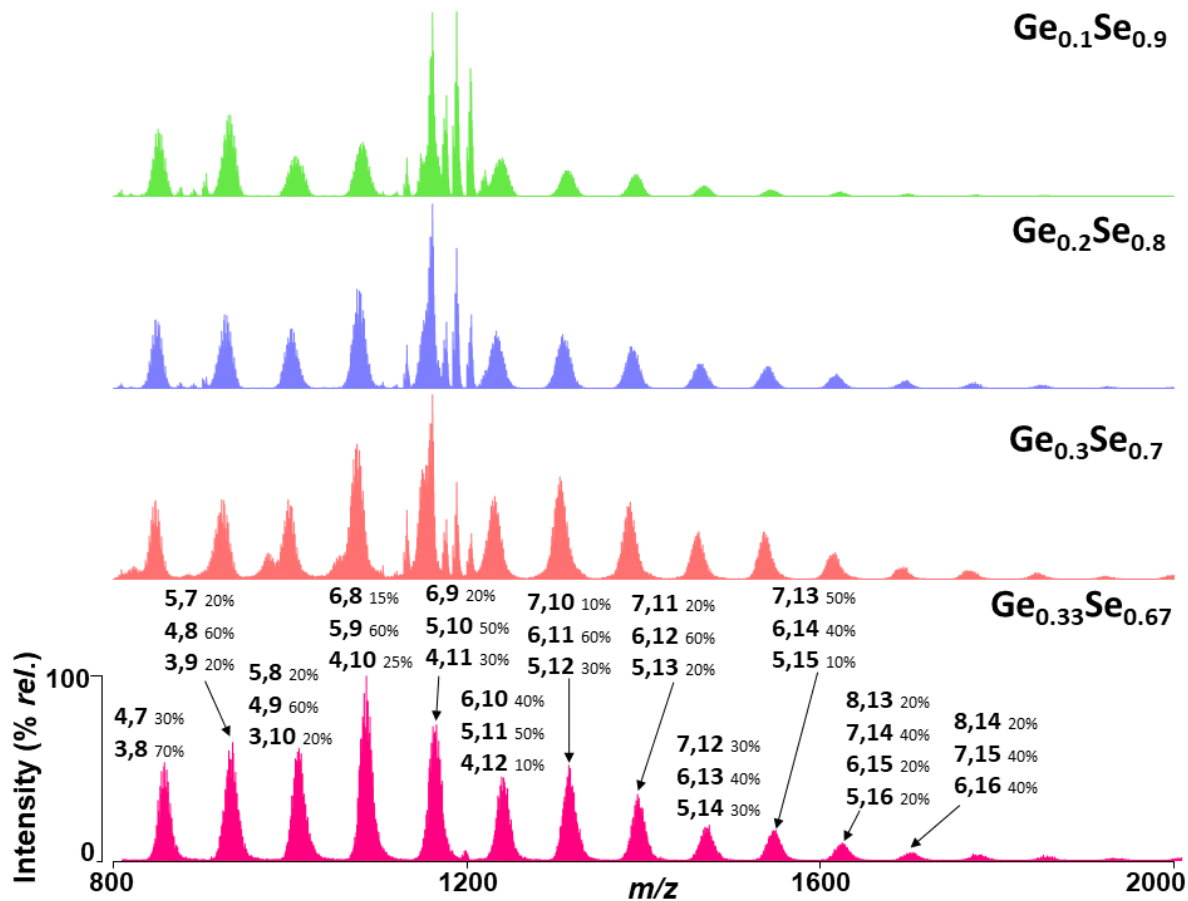


**Fig. 2:** Comparison of mass spectra obtained from all four bulk glass samples.

Conditions: positive ion mode, laser energy 160 a.u.

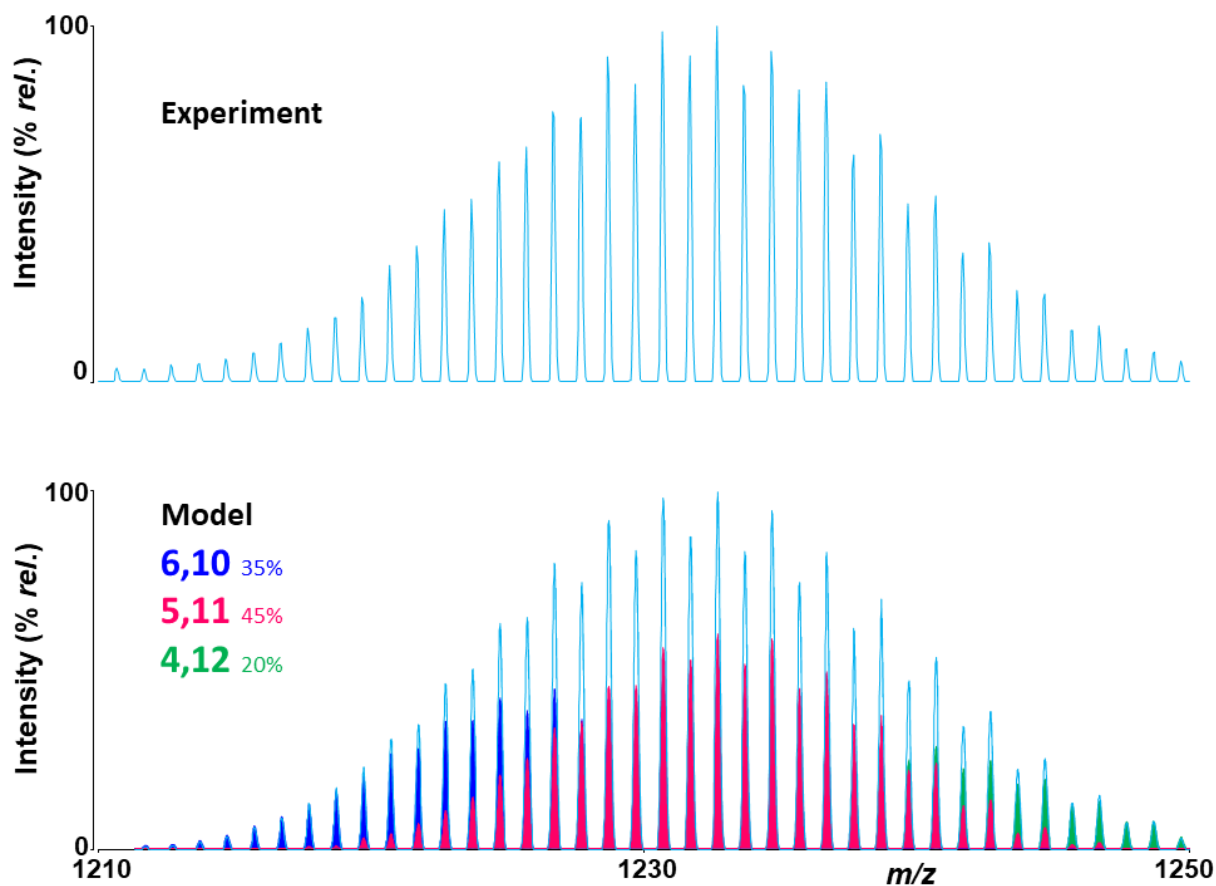


**Fig. 3:** Comparison of experimental and theoretical mass spectra obtained from  $\text{Ge}_{0.3}\text{Se}_{0.7}$ . Conditions: positive ion mode, laser energy 140 a.u.

In negative ion mode, the influence of laser energy was also studied and the threshold energy where the ionization initiated was found at  $\sim 120$  a.u. like for the positive ion mode. Increasing the laser energy up to 160 a.u. resulted in growing the intensity of the peaks but with a further increase in the laser energy the intensity decreased. This behavior is commonly observed for most of the samples at elevated laser energy, because of the decomposition of heavier mass clusters into small fragments. Fig. 4 shows the effect of laser energy on the mass spectra obtained from glass sample  $\text{Ge}_{0.1}\text{Se}_{0.9}$ .

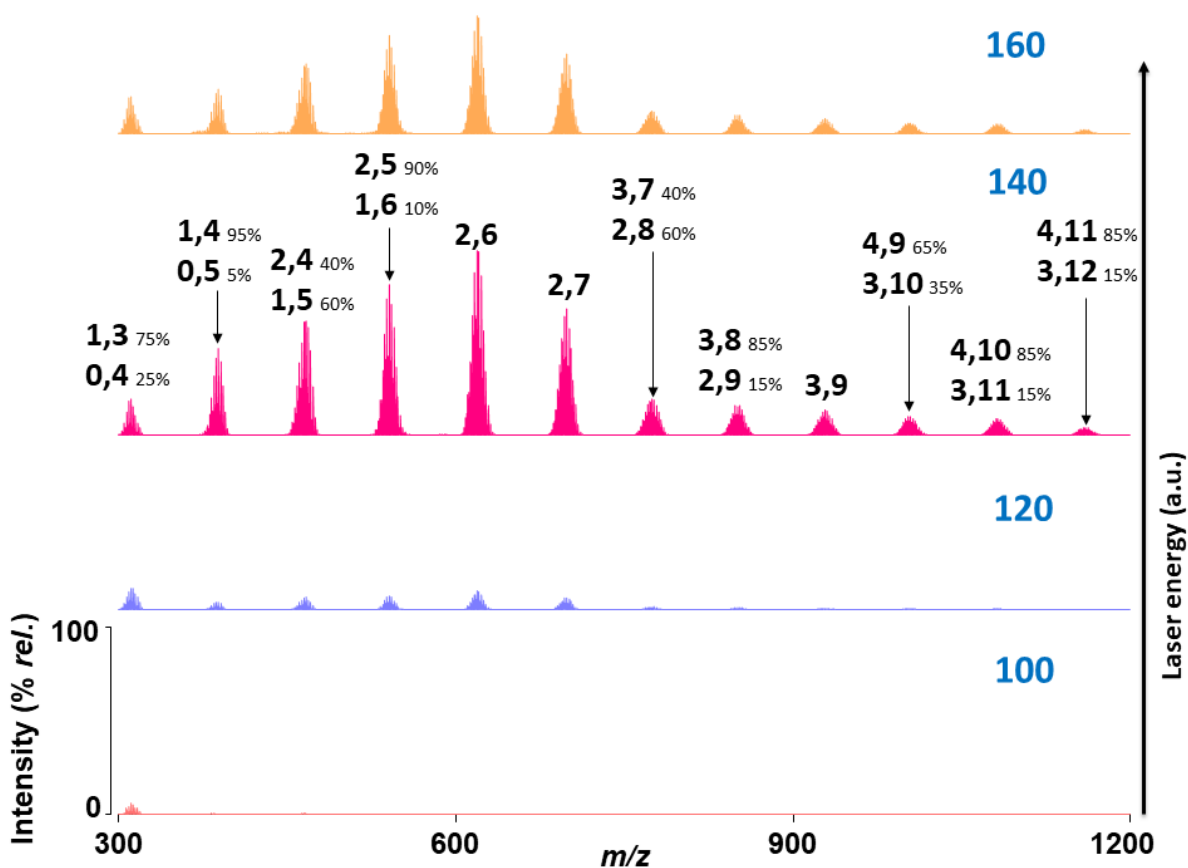


**Fig. 4:** The effect of laser energy on the LDI TOFMS of the sample  $\text{Ge}_{0.1}\text{Se}_{0.9}$ . Conditions: negative ion mode, laser energy 100-160 a.u. The mass spectra are normalized at peak intensity 244.

The “richest” mass spectra with respect to the highest number of clusters and highest peak intensities were obtained at laser energy  $\sim 140$ -160 a.u., which is similar to positive ion mode. Unary  $\text{Se}_b^-$  ( $b=2-4$ ),  $\text{Ge}_a^-$  ( $a=4, 7$ ), and many binary  $\text{Ge}_a\text{Se}_b^\pm$  clusters were detected. A list of all the clusters is given in Supplementary Table 3. The lowest mass cluster assigned (at measurement conditions) was  $\text{Se}_2^+$  for all the glass samples and the highest mass cluster detected was  $\text{Ge}_8\text{Se}_{14}^+$  which overlapped with  $\text{Ge}_7\text{Se}_{15}^+$  and  $\text{Ge}_6\text{Se}_{16}^+$  for  $\text{Ge}_{0.3}\text{Se}_{0.7}$  and  $\text{Ge}_{0.33}\text{Se}_{0.67}$ . Nevertheless, the intensity of highest mass cluster was quite low as compared to  $\text{Se}_2^+$ . Figs. 5 and 6 show the comparison of mass

spectra obtained from four bulk samples in the  $m/z$  range 200-1500 and 800-2000, respectively. The overlapping of the isotopic patterns with  $\geq 2$  species was detected, for example,  $\text{Se}_3^-$  (75%) +  $\text{GeSe}_2^-$  (25%);  $\text{Ge}_2\text{Se}_3^-$  (20%) +  $\text{GeSe}_4^-$  (80%);  $\text{Ge}_3\text{Se}_5^-$  (15%) +  $\text{Ge}_2\text{Se}_6^-$  (85%), etc. Their individual contributions (given in the brackets) to the overall isotopic pattern are different. The total numbers of species detected for individual samples are as follows: 37 for  $\text{Ge}_{0.1}\text{Se}_{0.9}$ , 40 for  $\text{Ge}_{0.2}\text{Se}_{0.8}$ , 49 for  $\text{Ge}_{0.3}\text{Se}_{0.7}$ , and 44 for  $\text{Ge}_{0.33}\text{Se}_{0.67}$ . Few more  $\text{Ge}_a\text{Se}_b^-$  species were observed but due to the low intensity and insufficient mass resolution, the stoichiometry of these clusters was not determined.

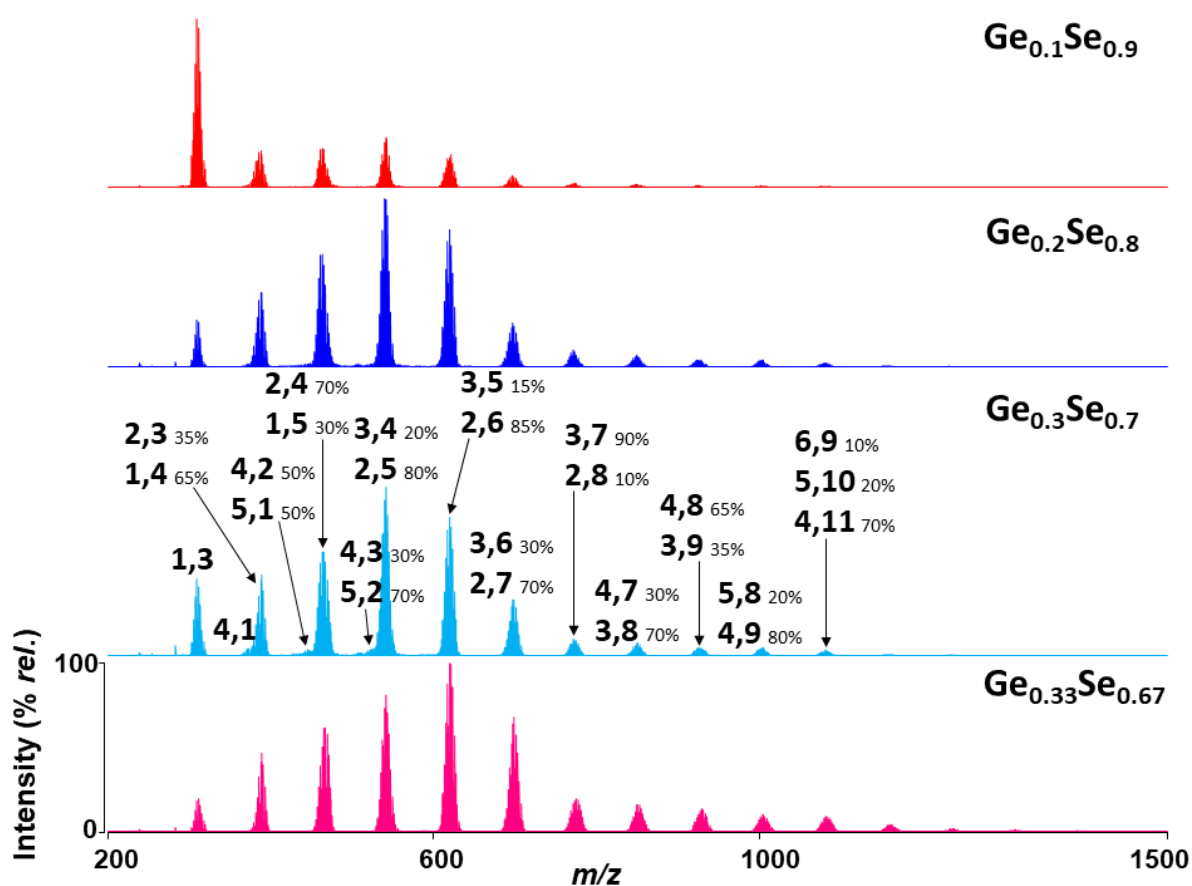


**Fig. 5:** Comparison of mass spectra obtained from all four bulk glass samples. Conditions: negative ion mode, range  $m/z$  200-1500, laser energy 160 a.u.

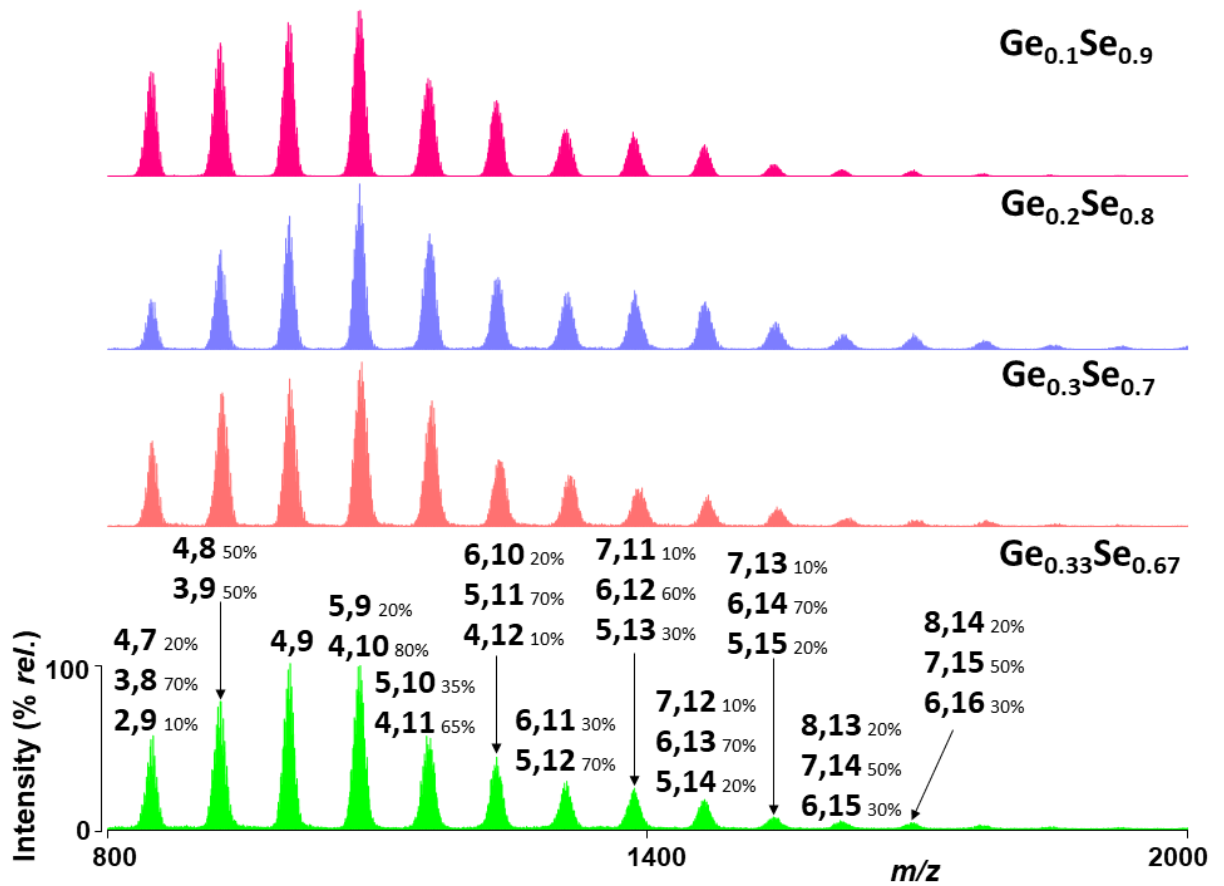


**Fig. 6:** Comparison of mass spectra obtained from all four bulk glass samples. Conditions: negative ion mode, range  $m/z$  800-2000, laser energy 160 a.u.

It was observed that the isotopic patterns of some clusters were shifted towards lower mass side as the amount of germanium in the bulk glass increases from 10-30 at.%, i.e. in the order  $\text{Ge}_{0.1}\text{Se}_{0.9} < \text{Ge}_{0.2}\text{Se}_{0.8} < \text{Ge}_{0.3}\text{Se}_{0.7}$ . Moreover, the contribution of the highest germanium containing species in the overall isotopic pattern increased in the same order of increasing the amount of germanium in the bulk samples. Such a shift was not seen between the samples  $\text{Ge}_{0.3}\text{Se}_{0.7}$  and  $\text{Ge}_{0.33}\text{Se}_{0.67}$ , this might be because of their small difference in the composition. This observation is illustrated in Supplementary Fig. S4.

We turn to the analysis of thin films prepared from  $\text{Ge}_{0.2}\text{Se}_{0.8}$  and  $\text{Ge}_{0.33}\text{Se}_{0.67}$  via magnetron sputtering. The ionization threshold energy for the thin films was found

somewhat lower as compared to the powdered bulk samples. In case of positive ion mode spectra, the threshold energy was about ~100-110 a.u. The “optimal” mass spectra were recorded at laser energy between 120 and 130 a.u. The lowest mass cluster detected is  $\text{GeSe}_2^+$  for both the thin film samples; the highest mass clusters are  $\text{Ge}_6\text{Se}_{13}^+$  (70%) overlapped with  $\text{Ge}_5\text{Se}_{14}^+$  (30%) and  $\text{Ge}_4\text{Se}_8^+$  (70%) overlapped with  $\text{Ge}_5\text{Se}_7^+$  (30%), for the  $\text{Ge}_{0.2}\text{Se}_{0.8}$  and  $\text{Ge}_{0.33}\text{Se}_{0.67}$  films, respectively. The further observed peaks were recognized as for  $\text{Ge}_{0.2}\text{Se}_{0.8}$  thin film:  $\text{Se}_2^+$ ,  $\text{GeSe}_4^+$ ; in addition, many other overlapped clusters were detected:  *$\text{Ge}_2\text{Se}_2^+$  (15%) overlapped with  $\text{GeSe}_3^+$ (75%) +  $\text{Se}_4^+$ (10%),  $\text{Ge}_2\text{Se}_4^+$  (60%) with  $\text{GeSe}_5^+$ (40%),  $\text{Ge}_3\text{Se}_4^+$  (35%) with  $\text{Ge}_2\text{Se}_5^+$ (55%) +  $\text{GeSe}_6^+$ (10%),  $\text{Ge}_3\text{Se}_5^+$  (10%) with  $\text{Ge}_2\text{Se}_6^+$ (40%) +  $\text{GeSe}_7^+$ (50%),  $\text{Ge}_4\text{Se}_5^+$  (10%) with  $\text{Ge}_3\text{Se}_6^+$ (90%),  $\text{Ge}_3\text{Se}_7^+$  (80%) with  $\text{Ge}_2\text{Se}_8^+$ (20%),  $\text{Ge}_4\text{Se}_7^+$  (10%) with  $\text{Ge}_3\text{Se}_8^+$ (80%) +  $\text{Ge}_2\text{Se}_9^+$ (10%),  $\text{Ge}_5\text{Se}_7^+$  (10%) with  $\text{Ge}_4\text{Se}_8^+$ (80%) +  $\text{Ge}_3\text{Se}_9^+$ (10%),  $\text{Ge}_5\text{Se}_8^+$  (20%) with  $\text{Ge}_4\text{Se}_9^+$  (80%) +  $\text{Ge}_3\text{Se}_{10}^+$ (20%),  $\text{Ge}_6\text{Se}_8^+$  (10%) with  $\text{Ge}_5\text{Se}_9^+$  (50%) +  $\text{Ge}_4\text{Se}_{10}^+$ (40%),  $\text{Ge}_6\text{Se}_9^+$  (10%) with  $\text{Ge}_5\text{Se}_{10}^+$ (40%) +  $\text{Ge}_4\text{Se}_{11}^+$  (50%),  $\text{Ge}_6\text{Se}_{10}^+$  (10%) with  $\text{Ge}_5\text{Se}_{11}^+$ (80%) +  $\text{Ge}_4\text{Se}_{12}^+$ (10%),  $\text{Ge}_6\text{Se}_{11}^+$  (30%) with  $\text{Ge}_5\text{Se}_{12}^+$ (70%),  $\text{Ge}_6\text{Se}_{12}^+$  (70%) with  $\text{Ge}_5\text{Se}_{13}^+$ (30%),  $\text{Ge}_6\text{Se}_{13}^+$  (70%) with  $\text{Ge}_5\text{Se}_{14}^+$ (30%).* For the  $\text{Ge}_{0.33}\text{Se}_{0.67}$  thin film, lower number of clusters was detected as compared to the above mentioned clusters. The clusters detected in LDI MS of both the thin films are indicated above in italics font, however it is noted that the percentage of overlapping is different for both samples. Apart from above described species,  $\text{Ge}_2\text{Se}_3^+$  and  $\text{Ge}_4\text{Se}_6^+$  clusters were identified. Additionally, several low intensity, unidentified peaks were detected.

When the Ge-Se thin films were examined in negative ion mode, threshold energy was found between 110 and 120 a.u. The lowest mass cluster was  $\text{Se}_2^-$  for both the samples, while the highest mass clusters for  $\text{Ge}_{0.2}\text{Se}_{0.8}$  are  $\text{Ge}_9\text{Se}_{18}^-$  and  $\text{Ge}_4\text{Se}_{10}^-$  (65%) overlapped with  $\text{Ge}_3\text{Se}_{11}^-$  (35%) for  $\text{Ge}_{0.33}\text{Se}_{0.67}$ . Some clusters such as  $\text{Se}_3^-$ ,  $\text{GeSe}_4^-$ ,  $\text{Ge}_2\text{Se}_4^-$ ,

$\text{Ge}_7\text{Se}_{16}^-$ ,  $\text{Ge}_8\text{Se}_{17}^-$  are not overlapped with any other species. The overlapped clusters recorded during LDI of  $\text{Ge}_{0.2}\text{Se}_{0.8}$  thin film are  *$\text{GeSe}_3^-$*  (70%) with  $\text{Se}_4^+$ (30%),  *$\text{Ge}_4\text{Se}_8^-$*  (20%) with  *$\text{Ge}_3\text{Se}_9^-$*  (30%) +  $\text{Ge}_2\text{Se}_{10}^-$  (50%),  $\text{Ge}_5\text{Se}_9^-$  (50%) with  *$\text{Ge}_4\text{Se}_{10}^-$*  (50%),  $\text{Ge}_6\text{Se}_{10}^-$  (70%) with  $\text{Ge}_5\text{Se}_{11}^-$  (30%).

The clusters observed in both the Ge-Se thin films are given above in italics font. Other than those were detected in LDI of  $\text{Ge}_{0.33}\text{Se}_{0.67}$  thin film:  $\text{Ge}_3\text{Se}_8^-$ ,  $\text{GeSe}_{11}^-$ ,  *$\text{Ge}_4\text{Se}_8^-$*  (30%) with  *$\text{Ge}_3\text{Se}_9^-$*  (50%) +  $\text{GeSe}_{11}^-$  (20%),  $\text{Ge}_4\text{Se}_{10}^-$  (65%) overlapped with  $\text{Ge}_3\text{Se}_{11}^-$  (35%),  $\text{Ge}_3\text{Se}_5^-$  (50%) overlapped with  $\text{Ge}_2\text{Se}_6^+$  (50%),  $\text{Ge}_3\text{Se}_6^-$  (15%) overlapped with  $\text{Ge}_2\text{Se}_7^+$  (85%),  $\text{Ge}_5\text{Se}_8^-$  (35%) overlapped with  $\text{Ge}_4\text{Se}_9^-$  (65%). No clusters were detected over  $m/z$  1000.

From the above results, it is noticed that the number of species generated via LDI in plasma phase for the  $\text{Ge}_{0.33}\text{Se}_{0.67}$  thin film is lower than for the  $\text{Ge}_{0.2}\text{Se}_{0.8}$  one. This is contrary to the case of bulk glasses, where, the highest number of clusters was detected for the  $\text{Ge}_{0.33}\text{Se}_{0.67}$ .

#### 4.3. Ge-Se bulk glass powders dispersed in parafilm

It is well known that LDI is considered a destructive method. From the results obtained in our previous work [26], we have concluded that the LDI breaks the original structure of the glasses, yielding small fragments which might partly originate from real glass structure. Therefore, one can say that some part of the generated clusters is a result of the fragmentation of glass structure. Also, some synthetic reactions between individual species probably take place due to their high energy. In spite of that, identified species give partial information about the structure of the studied materials. We have proved [26] that the use of some materials, such as a solution of parafilm and polymers like polyethylene glycol and polyvinylpyrrolidone may increase the number of species

observed in the mass spectra. Especially, the solution of parafilm was found to be more effective for this purpose. Therefore, here we have applied the same methodology using a solution of parafilm in this study.

Powdered  $\text{Ge}_x\text{Se}_{1-x}$  ( $x = 0.1, 0.2, 0.3, 0.33$ ) chalcogenide glass samples were dispersed in the parafilm solution [prepared by dissolving a piece ( $1 \text{ cm} \times 1 \text{ cm}$ ) of parafilm in xylene (1 ml)], deposited onto the target, dried and then examined by LDI TOFMS in a similar way as described for the Ge-Se glass powdered samples.

Many new, higher mass clusters in both positive and negative ion modes were identified using the method described above. The intensity of the peaks (detected within both methods of measurements) was enhanced in most of the cases when the parafilm was used. The intensity of peaks concerning new high mass clusters is rather low; as a result stoichiometry of some new species was not identified. The highest number of new heavier clusters was identified for the  $\text{Ge}_{0.33}\text{Se}_{0.67}$  sample in both, positive (22) and negative (5) ion modes (For the comparison of mass spectra obtained from  $\text{Ge}_{0.33}\text{Se}_{0.67}$  with and without parafilm in negative ion mode c.f. Supplementary Fig. S5). The comparison of mass spectra in positive ion mode obtained for  $\text{Ge}_{0.33}\text{Se}_{0.67}$  with and without parafilm solution is given in Fig. 7. In addition to the above-mentioned clusters,  $\text{Ge}_3\text{Se}_4^-$ ,  $\text{Ge}_5\text{Se}_8^-$ ,  $\text{Ge}_4\text{Se}_5^+$  new species were detected. For  $\text{Ge}_{0.1}\text{Se}_{0.9}$  in positive ion mode, no new heavier cluster was detected, while only one was assigned in negative ion mode. However, many new germanium rich  $\text{Ge}_a\text{Se}_b^{+/-}$  clusters such as  $\text{Ge}_4\text{Se}^-$ ,  $\text{Ge}_4\text{Se}_2^-$ ,  $\text{Ge}_5\text{Se}_2^-$ ,  $\text{Ge}_5\text{Se}_3^-$ ,  $\text{Ge}_8\text{Se}^-$ ,  $\text{Ge}_6\text{Se}_3^-$ ,  $\text{Ge}_5\text{Se}_4^-$ ,  $\text{Ge}_9\text{Se}^-$ , and  $\text{Ge}_6\text{Se}_4^-$ , in addition to pure germanium clusters like  $\text{Ge}_7^-$  and  $\text{Ge}_8^-$  were found. For  $\text{Ge}_{0.2}\text{Se}_{0.8}$  dispersed in parafilm, new species such as  $\text{GeSe}_3^+$ ,  $\text{Se}_5^+$ ,  $\text{Ge}_3\text{Se}_{11}^+$ ,  $\text{Ge}_6\text{Se}_{10}^+$  (non-overlapped),  $\text{Ge}_8\text{Se}_{15}^+$  overlapped with [ $\text{Ge}_7\text{Se}_{16}^+$ ,  $\text{Ge}_6\text{Se}_{17}^+$ ],  $\text{Ge}_8\text{Se}_{16}^+$  overlapped with [ $\text{Ge}_7\text{Se}_{17}^+$ ,  $\text{Ge}_6\text{Se}_{18}^+$ ],  $\text{Ge}_8\text{Se}_{17}^+$  overlapped with [ $\text{Ge}_7\text{Se}_{18}^+$ ,  $\text{Ge}_6\text{Se}_{19}^+$ ] in positive ion mode, while,  $\text{Ge}_5\text{Se}^-$  overlapped

with  $\text{Ge}_4\text{Se}_2^-$ ,  $\text{Ge}_5\text{Se}_2^-$  overlapped with  $\text{Ge}_4\text{Se}_3^-$ ,  $\text{Ge}_7\text{Se}_{15}^-$  overlapped with  $\text{Ge}_6\text{Se}_{16}^-$ ,  $\text{Ge}_7\text{Se}_{16}^-$  overlapped with  $\text{Ge}_6\text{Se}_{17}^-$  and some non-overlapped  $\text{Ge}_4^-$ ,  $\text{Ge}_5\text{Se}_3^-$ ,  $\text{Ge}_3\text{Se}_5^-$ ,  $\text{Ge}_3\text{Se}_6^-$ ,  $\text{Ge}_5\text{Se}_{16}^-$  species were detected in negative ion mode. The new clusters observed in positive and negative ion modes when performing LDI TOFMS of  $\text{Ge}_{0.3}\text{Se}_{0.7}$  glass powder dispersed in parafilm solution are:  $\text{GeSe}_3^+$ ,  $\text{Ge}_6\text{Se}_7^+$ ,  $\text{Ge}_3\text{Se}_{10}^+$ ,  $\text{Ge}_5\text{Se}_{16}^+$ ,  $\text{GeSe}_2^-$ ,  $\text{Ge}_4^-$ ,  $\text{Ge}_3\text{Se}_2^-$ ,  $\text{GeSe}_7^-$ ,  $\text{Ge}_7\text{Se}_{11}^-$ ;  $\text{Ge}_8\text{Se}_{15}^+$  overlapped with  $[\text{Ge}_7\text{Se}_{16}^+, \text{Ge}_6\text{Se}_{17}^+]$ ,  $\text{Ge}_6\text{Se}_2^-$  overlapped with  $\text{Ge}_5\text{Se}_3^-$ . A complete overview of clusters detected when the powdered glass samples were dispersed in parafilm solution is given in Supplementary Table 2 and 3 for positive and negative ion modes, respectively.

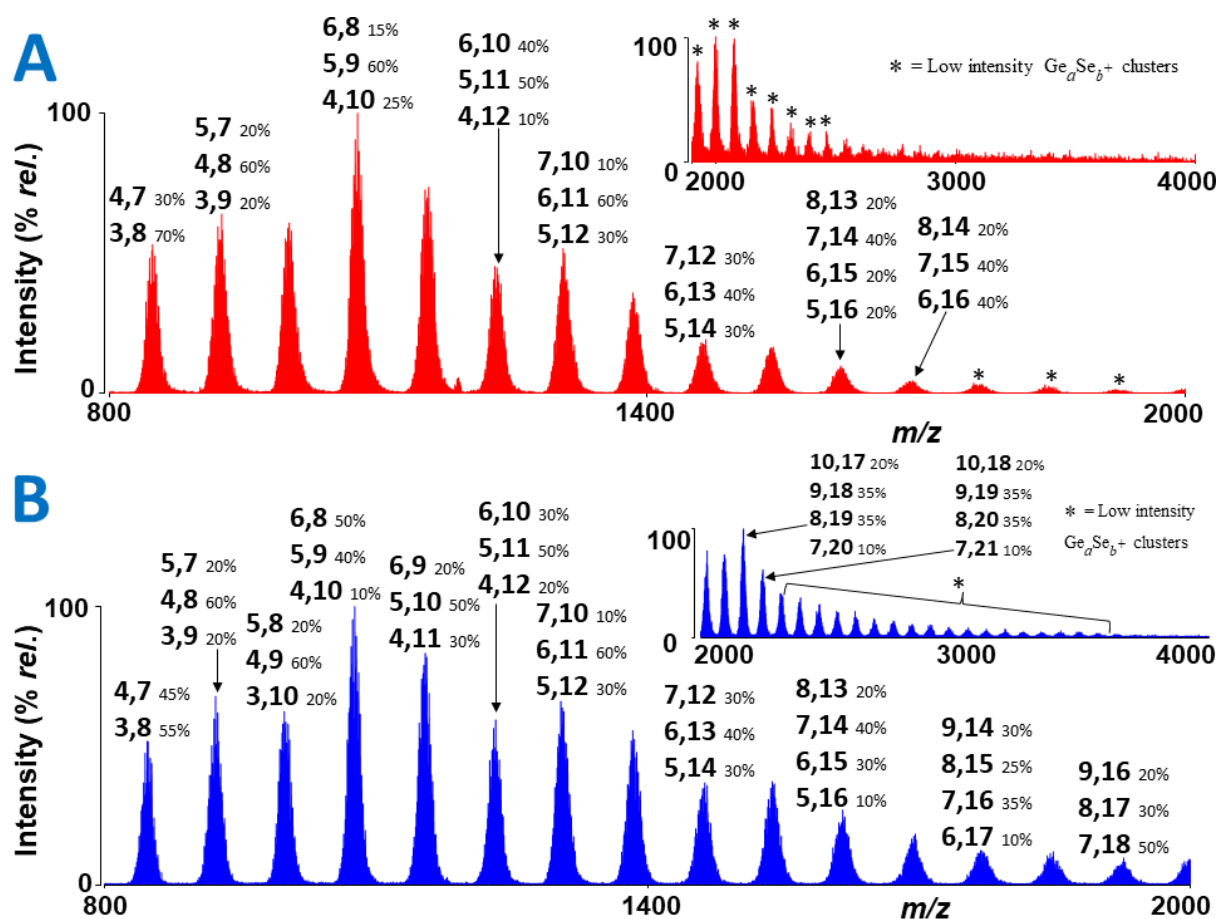


Fig. 7: Comparison of mass spectra obtained from A)  $\text{Ge}_{0.33}\text{Se}_{0.67}$ , B)  $\text{Ge}_{0.33}\text{Se}_{0.67}$  dispersed in the parafilm solution. Conditions: laser energy 140 a.u., positive ion mode. For the sake of clarity, description of a few peaks is given.

The local structure of Ge-Se glasses can be determined on the basis of Raman scattering spectra [30,36–38]. According to the Raman spectra, the corner and edge-sharing  $\text{GeSe}_4$  tetrahedral units are present in the structure of Ge-Se glasses [28,36,38]. Also the signatures of Se-Se, Ge-Ge bond were identified [29]. LDI TOFMS results might evidence at least some of the structural units identified in Raman spectra. For example, observed  $\text{GeSe}_4^{+/-}$ ,  $\text{Ge}_2\text{Se}_8^{+/-}$ ,  $\text{Ge}_3\text{Se}_{12}^{+/-}$ ,  $\text{Ge}_4\text{Se}_{16}^{+/-}$  clusters confirm the presence of  $\text{GeSe}_4$  tetrahedral entities in the structure of the Ge-Se glasses. It is worth to note that these  $(\text{GeSe}_4)_n^{+/-}$  ( $n= 1-4$ ) clusters were observed only in the  $\text{Ge}_{0.1}\text{Se}_{0.9}$  and  $\text{Ge}_{0.2}\text{Se}_{0.8}$  glasses, where the selenium is present in large excess, while for other two glasses only  $\text{GeSe}_4^{+/-}$  was detected. The other low mass species such as  $\text{GeSe}_2^{+/-}$ ,  $\text{GeSe}_3^{+/-}$ ,  $\text{GeSe}_5^{+/-}$ ,  $\text{GeSe}_6^{+/-}$ , etc. are probably formed either by the i) fragmentation of  $\text{GeSe}_4^{+/-}$  and  $\text{Ge}_2\text{Se}_8^{+/-}$ , respectively or ii) could be formed by the reactions proceeding in plasma due highly energetic ions and clusters. Similarly, the other lighter mass species might be formed from  $\text{Ge}_3\text{Se}_{12}^{+/-}$ ,  $\text{Ge}_4\text{Se}_{16}^{+/-}$ . Moreover, the existence of Se-Se and Ge-Ge homopolar bonds in Raman spectra of Ge-Se glasses are also evidenced, for example by the presence of  $\text{Se}_b^{+/-}$  ( $b = 2-5$ ),  $\text{Ge}_2\text{Se}_4^{+/-}$ ,  $\text{Ge}_2\text{Se}_6^{+/-}$ , and  $\text{Ge}_4^-$ ,  $\text{Ge}_7^-$ ,  $\text{Ge}_8^-$  clusters. Some of the higher mass clusters which could not be considered as a part of the Ge-Se glass structure such as  $\text{Ge}_8\text{Se}_{13}^{+/-}$ ,  $\text{Ge}_8\text{Se}_{15}^{+/-}$ ,  $\text{Ge}_7\text{Se}_{16}^{+/-}$ ,  $\text{Ge}_7\text{Se}_{21}^{+/-}$ ,  $\text{Ge}_8\text{Se}_{20}^{+/-}$ ,  $\text{Ge}_9\text{Se}_{19}^{+/-}$ , etc. could be formed by the laser ablation synthesis due to energetic species present in the plasma plume.

Considering the MS data obtained in different  $m/z$  ranges, the most intensive signals were obtained predominantly for  $\text{Se}_2^+$ ,  $\text{GeSe}_2^+$ , and  $\text{GeSe}_4^+$  in positive ion mode and  $\text{Se}_2^-$ ,  $\text{Se}_3^-$ ,  $\text{Ge}_2\text{Se}_5^-$ , and  $\text{Ge}_2\text{Se}_6^-$  in negative ion mode.

It is noted that for all the mass spectra, the number of germanium and germanium rich  $\text{Ge}_a\text{Se}_b^{+/-}$  species is significantly low as compared to the number of selenium-rich

species. This fact could probably be explained by the difficult ionization of the germanium clusters [25]. The results of this work are qualitatively comparable to our previously published results from  $(\text{GeSe}_2)_{100-x}(\text{Sb}_2\text{Se}_3)_x$  system, where we have faced the problem of ionization of germanium and germanium-rich species [29]. Unfortunately, from the mass spectra, quantitative evaluation of species generated during LDI is difficult to obtain due to the fact that accurate correlation between measured mass spectrometric signals and the total number of generated ions are not known.

To have a more complex picture of the Ge-Se glasses and thin films, we performed also SNMS measurements. An example of SNMS results is given in Fig. 8, which shows the mass spectrum of  $\text{Ge}_{0.33}\text{Se}_{0.67}$  bulk glass. All the SNMS data were recalculated quantitatively in order to get neutrals composition of the studied glasses and films. Even if the calculation of chemical composition in this way may present error bars of 5-8 at. %, SNMS clearly confirms that the composition of the neutrals follows qualitatively the nominal composition of materials under study. Nevertheless, to be completely sure that the low intensities of germanium and germanium rich  $\text{Ge}_a\text{Se}_b^{+/-}$  species in LDI TOFMS data originate in difficulties during ionization of such clusters, secondary ion mass spectrometry experiments are planned in near future.

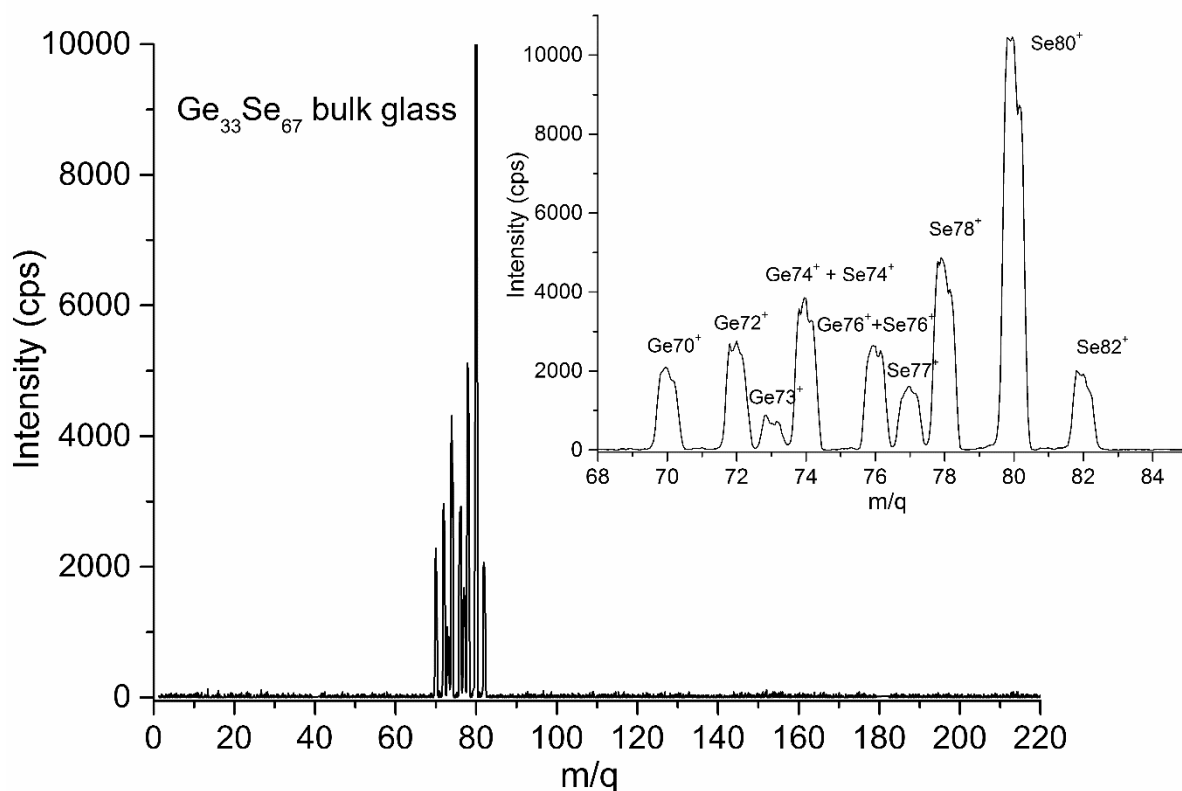


**Fig. 8:** Secondary neutral mass spectra of  $\text{Ge}_{0.33}\text{Se}_{0.67}$  bulk glass. The inset presents a detail of the spectra for  $m/q$  range of 68-85.

When the solution of parafilm was used for the dispersion of Ge-Se glass powders, many new, high mass clusters were detected as compared to mass spectra of simple Ge-Se powders. This can be explained by the two hypotheses. First, parafilm is playing a kind of protecting role leading to lower fragmentation of original glass structure due to the interaction of high energy laser pulses. The second reason for the observation of high mass clusters (when using parafilm medium for LDI TOFMS) might be its pronouncing effect on the laser ablation synthetic reactions of lighter plasma species. Whatever the case, the conclusion is that some more complex structures in the form of higher mass clusters are generated when using polymers.

When the results obtained for mass spectra of Ge-Se mixtures and glasses were compared, it was noted that a very high number of species was generated in case of LDI TOFMS of glasses. The glasses were fabricated through high-temperature synthesis and proceeding reactions formed a complex 3D structure. Consequently, when the glasses are irradiated with laser pulses, the clusters can be formed either by fragmentation of original local structure or by reactions of energetic ions present in plasma plume, i.e. by laser ablation synthesis. In the case of the Ge-Se elemental mixtures in which germanium and selenium were not reacted with each other before their exposure to the laser pulses, the clusters were generated probably by only laser ablation synthesis itself.

Unfortunately, despite of all accessible data, we think that due to complexity of laser ablation processes, it is probably impossible to find simple correlation between species observed in this work and the parameters of the deposited films.

## 5. Conclusions

LDI TOFMS was applied for the generation and study of clusters from Ge-Se chalcogenide glasses and their thin films. Approximately about 50 different unary and binary ( $\text{Ge}_a^{+/-}$ ,  $\text{Se}_b^{+/-}$ , and  $\text{Ge}_a\text{Se}_b^{+/-}$ ) species were generated for each glass sample. The clusters generated are either formed due to the deeper fragmentation of original glass structure or some high mass species which are not considered as the part of original glass structure can be formed from the highly energetic ions present in the plasma plume, i.e. by laser ablation synthesis. When using parafilm for the dispersion of chalcogenide glass powders, many new, high mass clusters were generated. On the other hand, when performing LDI TOFMS experiments with simple elemental Ge-Se mixtures, much lower variety of species was found which seems to be connected with the fact that the

mixtures (contrary to glasses) have no original 3D structure and thus all clusters are formed only by laser ablation synthesis.

To conclude, the results obtained are helpful for understanding the processes proceeding in plasma plume due to the interaction of laser pulses with solid state materials. Also, determination of stoichiometry of the clusters generated via LDI TOFMS is useful for the partial structural characterization of chalcogenide glasses and their thin films. Finally, the parafilm used here can widen the applications of LDI for other materials.

## **Acknowledgments**

The authors are grateful to the Czech Science Foundation (project no. 18-03823S) for supporting this work. This research has been also supported by CEPLANT, the project R&D center for low-cost plasma and nanotechnology surface modifications CZ.1.05/2.1.00/03.0086 funded by European Regional Development Fund and the Projects CZ.1.07/2.3.00/30.0058 and LM2015082 of the Ministry of Education, Youth, and Sports of the Czech Republic.

## References

- [1] J.-L. Adam, X. Zhang, eds., Chalcogenide Glasses Preparation, Properties and Applications, Woodhead Publishing Ltd, 2013.
- [2] S. Song, N. Carlie, J. Boudies, L. Petit, K. Richardson, C.B. Arnold, Spin-coating of  $\text{Ge}_{23}\text{Sb}_7\text{S}_{70}$  chalcogenide glass thin films, *J. Non. Cryst. Solids* 355 (2009) 2272–2278.
- [3] X. Song, W. Zhou, X. Liu, Y. Gu, S. Zhang, Layer-controlled band alignment, work function and optical properties of few-layer GeSe, *Phys. B Condens. Matter*. 519 (2017) 90–94.
- [4] Y. Wang, S. Qi, Z. Yang, R. Wang, A. Yang, P. Lucas, Composition dependences of refractive index and thermo-optic coefficient in Ge-As-Se chalcogenide glasses, *J. Non. Cryst. Solids* 459 (2017) 88–93.
- [5] N. Afify, Structural relaxation of  $\text{GeSe}_2$  chalcogenide glass studied with use of the radial distribution function, *Phys. Rev. B*. 48 (1993) 16304–16309.
- [6] X. Zhang, J. Shen, S. Lin, J. Li, Z. Chen, W. Li, Y. Pei, Thermoelectric properties of GeSe, *J. Mater.* 2 (2016) 331–337.
- [7] H.Y. Zhao, Y.P. Koh, M. Pyda, S. Sen, S.L. Simon, The kinetics of the glass transition and physical aging in germanium selenide glasses, *J. Non. Cryst. Solids* 368 (2013) 63–70.
- [8] Z. Li, M. Liu, Q. Chen, Y. Huang, C. Cao, Y. He, The electronic structure of GeSe monolayer with light nonmetallic elements decoration, *Superlattices Microstruct.* 109 (2017) 829–840.
- [9] J.H. Lee, J.H. Yi, W.H. Lee, B.J. Park, Y.G. Choi, Crystallization behavior of Ge-Sb-Se glasses in the compositional range for use as molded lenses, *J. Non. Cryst. Solids*. 481 (2018) 21–26.
- [10] L. Petit, N. Carlie, H. Chen, S. Gaylord, J. Massera, G. Boudebs, J. Hu, A. Agarwal, L. Kimerling, K. Richardson, Compositional dependence of the nonlinear refractive index of new germanium-based chalcogenide glasses, *J. Solid State Chem.* 182 (2009) 2756–2761.
- [11] M.M. Abdel-Aziz, Effect of Thallium on the Crystallization Kinetics of the Chalcogenide Glasses  $\text{GeSe}_2$  and  $\text{GeSe}_4$ , *J. Therm. Anal.* 79 (2005) 709–714.
- [12] P. Li, Y. Zhang, Z. Chen, P. Gao, T. Wu, L.M. Wang, Relaxation dynamics in the strong

- chalcogenide glass-former of  $\text{Ge}_{22}\text{Se}_{78}$ , *Sci. Rep.* 7 (2017) 1–8.
- [13] M. Cobb, D.A. Drabold, R.L. Cappelletti, Ab initio molecular-dynamics study of the structural, vibrational, and electronic properties of glassy  $\text{GeSe}_2$ , *Phys. Rev. B.* 54 (1996) 162–171.
- [14] T. Grande, M. Ishii, M. Akaishi, S. Aasland, Structural Properties of  $\text{GeSe}_2$  at High Pressures, *J. Solid State Chem.* 173 (1999) 167–173.
- [15] M. Kibalchenko, J.R. Yates, C. Massobrio, A. Pasquarello, Structural Composition of First-Neighbor Shells in  $\text{GeSe}_2$  and  $\text{GeSe}_4$  Glasses from a First-Principles Analysis of NMR Chemical Shifts, *J. Phys. Chem. C.* 115 (2011) 7755–7759.
- [16] P. Klocek, L. Colombo, Index of refraction, dispersion, bandgap and light scattering in  $\text{GeSe}$  and  $\text{GeSbSe}$  glasses, *J. Non. Cryst. Solids* 93 (1987) 1–16.
- [17] P.S. Salmon, I. Petri, Structure of glassy and liquid  $\text{GeSe}_2$  Structure of glassy and liquid  $\text{GeSe}_2$ , *J. Phys. Condens. Matter.* 15 (2003) S1509–S1528.
- [18] P. Armand, A. Ibanez, Q. Ma, D. Raoux, E. Philippot, Structural characterization of germanium selenide glasses by differential anomalous X-ray scattering, *J. Non. Cryst. Solids.* 167 (1993) 37–49.
- [19] B.H. Eckert, Structural Characterization of Non-Oxide Chalcogenide Glasses using Solid State NMR, *Adv. Mater.* 101 (1989) 1763–1772.
- [20] P. Tronc, M. Bensoussan, A. Brenac, Optical-Absorption Edge and Raman Scattering in  $\text{Ge}_x\text{Se}_{1-x}$  glasses, *Phys. Rev. B.* 8 (1973) 5947–5956.
- [21] L.F. Santos, A. Ganjoo, H. Jain, R.M. Almeida, Optical and spectroscopic characterization of germanium selenide glass films, *J. Non. Cryst. Solids* 355 (2009) 1984–1988.
- [22] S. Sen, Z. Gan, Chemical order around Ge atoms in binary germanium selenide glasses: Results from  $^{73}\text{Ge}$  solid-state NMR spectroscopy at 19.6 Tesla, *J. Non. Cryst. Solids* 356 (2010) 1519–1521.
- [23] R. Holomb, V. Mitsa, E. Akalin, S. Akyuz, M. Sichka, Ab initio and Raman study of medium range ordering in  $\text{GeSe}_2$  glass, *J. Non. Cryst. Solids.* 373–374 (2013) 51–56.
- [24] S. Pangavhane, P. Němec, T. Wagner, J. Janca, J. Havel, Laser desorption ionization time-of-

- flight mass spectrometric study of binary As-Se glasses, *Rapid Commun. Mass Spectrom.* 24 (2010) 2000–2008.
- [25] S.D. Pangavhane, P. Nemeč, V. Nazabal, A. Moreac, P. Jóvári, J. Havel, Laser desorption ionization time-of-flight mass spectrometry of erbium-doped Ga-Ge-Sb-S glasses, *Rapid Commun. Mass Spectrom.* 28 (2014) 1221–1232.
- [26] R.M. Mawale, M.V. Ausekar, L. Prokeš, V. Nazabal, E. Baudet, T. Halenkovič, M. Bouška, M. Alberti, P. Němec, J. Havel, Laser Desorption Ionization of  $\text{As}_2\text{Ch}_3$  (Ch = S, Se, and Te) Chalcogenides Using Quadrupole Ion Trap Time-of-Flight Mass Spectrometry: A Comparative Study, *J. Am. Soc. Mass Spectrom.* 3 (2017) 2569–2579.
- [27] K. Šútorová, P. Hawlová, L. Prokeš, P. Němec, R. Boidin, J. Havel, Laser desorption ionization time-of-flight mass spectrometry of Ge-As-Te chalcogenides, *Rapid Commun. Mass Spectrom.* 29 (2015) 408–414.
- [28] K. Šútorová, L. Prokeš, V. Nazabal, E. Baudet, J. Havel, P. Němec, Laser Desorption Ionization Time-of-Flight Mass Spectrometry of Glasses and Amorphous Films from Ge–As–Se System, *J. Am. Ceram. Soc.* 99 (2016) 3594–3599.
- [29] K. Šútorová, L. Prokeš, V. Nazabal, M. Bouška, J. Havel, P. Němec, Laser Desorption Ionisation Time-of-Flight Mass Spectrometry of Chalcogenide Glasses from  $(\text{GeSe}_2)_{100-x}(\text{Sb}_2\text{Se}_3)_x$  System, *J. Am. Ceram. Soc.* 98 (2015) 4107–4110.
- [30] V. Nazabal, F. Charpentier, J.-L. Adam, P. Nemeč, H. Lhermite, M.-L. Brandily-Anne, J. Charrier, J.-P. Guin, A. Moréac, Sputtering and Pulsed Laser Deposition for Near- and Mid-Infrared Applications: A Comparative Study of  $\text{Ge}_{25}\text{Sb}_{10}\text{S}_{65}$  and  $\text{Ge}_{25}\text{Sb}_{10}\text{Se}_{65}$  Amorphous Thin Films, *Int. J. Appl. Ceram. Technol.* 8 (2011) 990–1000.
- [31] T. Halenkovič, J. Gutwirth, P. Němec, E. Baudet, M. Specht, Y. Gueguen, J.C. Sangleboeuf, V. Nazabal, Amorphous Ge-Sb-Se thin films fabricated by co-sputtering: Properties and photosensitivity, *J. Am. Ceram. Soc.* 101 (2018) 2877–2887.
- [32] K. Sladkova, J. Houska, J. Havel, Laser desorption ionization of red phosphorus clusters and their use for mass calibration in time-of-flight mass spectrometry, *Rapid Commun. Mass Spectrom.* 23 (2009) 3114–3118.

- [33] D.D. Vaughn, R.J. Patel, M.A. Hickner, R.E. Schaak, Single-crystal colloidal nanosheets of GeS and GeSe, *J. Am. Chem. Soc.* 132 (2010) 15170–15172.
- [34] P. Hawlová, F. Verger, V. Nazabal, R. Boidin, P. Němec, Photostability of pulsed laser deposited amorphous thin films from Ge-As-Te system, *Sci. Rep.* 5 (2015) 9310.
- [35] P. Hawlová, F. Verger, V. Nazabal, R. Boidin, P. Němec, Accurate Determination of Optical Functions of Ge-As-Te Glasses via Spectroscopic Ellipsometry, *J. Am. Ceram. Soc.* 97 (2014) 3044–3047.
- [36] S. Sugai, Stochastic random network model in Ge and Si chalcogenide glasses, *Phys. Rev. B.* 35 (1987) 1345–1361.
- [37] K. Murase, T. Fukunaga, K. Yakushiji, Investigation of stability of (Ge, Sn)-(S, or Se)<sub>4/2</sub> cluster vibrational spectra, *J. Non. Cryst. Solids.* 60 (1983) 883–886.
- [38] K. Jackson, A. Briley, S. Grossman, D. V. Porezag, M.R. Pederson, Raman-active modes of a-GeSe<sub>2</sub> and a-GeS<sub>2</sub>: A first-principles study, *Phys. Rev. B - Condens. Matter Mater. Phys.* 60 (1999) R14985–R14989.